Supporting Information

# Application of flow-type electrochemical lithium recovery system with $\lambda$-$MnO_2$/$LiMn_2O_4$: Experiment and simulation

Hwajoo Joo[†, ǁ], Seon Yeop Jung[†, ǁ], Seoni Kim[†], Kyung Hyun Ahn[†], Won Sun Ryoo[‡], Jeyong Yoon[†, §, *]

[†]School of Chemical and Biological Engineering, College of Engineering, Institute of Chemical Processes (ICP), Seoul National University (SNU), 1 Gwanak-ro, Gwanak-gu, Seoul 08826, Republic of Korea.

[‡]Department of Chemical Engineering, Hongik University, Wausan-ro, Mapo-gu, Seoul 04066, Republic of Korea.

[§]Korea Environment Institute, 370 Sicheong-daero, Sejong-si 30147, Republic of Korea.

[*]Corresponding author's email: jeyong@snu.ac.kr

[ǁ]These authors contributed equally to this work.

*Number of pages: 9 (from S1 to S9)*

*Number of Figures: 5*

***Electrochemical characterization of $LiMn_2O_4$ electrode***

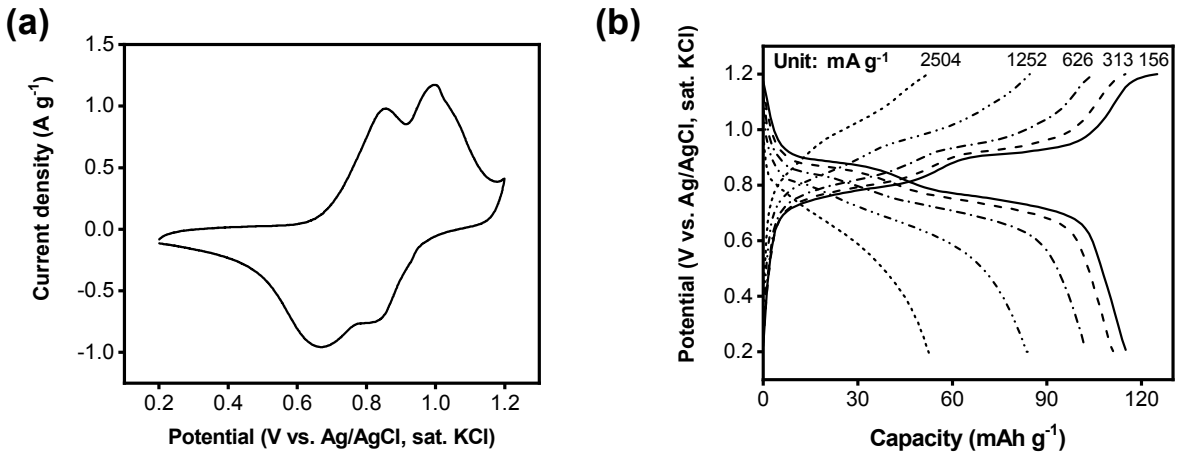


**Figure S1.** (a) Cyclic voltammetry (scan rate: 1 mV $s^{-1}$) and (b) galvanostatic charge/discharge test for the $LiMn_2O_4$ electrode in 1 M LiCl (current density: 156, 313, 626, 1252, 2504 mA $g^{-1}$).

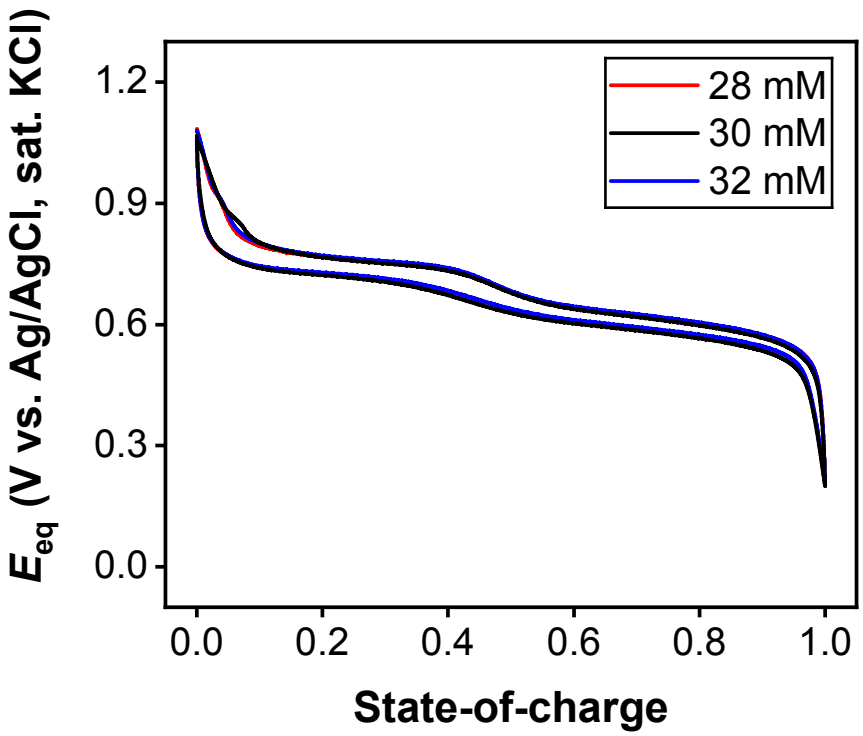


**Figure S2.** Change of the equilibrium potential ($E_{eq}$) of $\lambda$-$MnO_2$ ($LiMn_2O_4$) over State-of-charge. Measurement was conducted by galvanostatic discharge/charge test using 3-electrode cell (working: $\lambda$-$MnO_2$, counter: $LiMn_2O_4$, and reference: Ag/AgCl/KCl saturated) at $2.50\times10^{-1}$ mA $cm^{-2}$. 28, 30, and 32 mM LiCl aqueous solution was used as electrolyte.

**Figure S2** shows the equilibrium potentials of $\lambda$-$MnO_2$ ($LiMn_2O_4$) electrode as LiCl aqueous solution varied from 28 to 32 mM. The equilibrium potential shift appeared to be negligible in this range of concentration. The dependence of the equilibrium potential on the lithium ion concentration was excluded in the model.

## *Simulation details*

In the separator channel domain ($\Omega_s$), where a dilute LiCl solution is injected, $\varepsilon_i$ is set to unity ($\varepsilon_i = 1$) and no additional reaction is assumed ($S_i = 0$), which yields a mass transport problem without source term. To calculate the convective transport of the ion, a laminar flow field of the Newtonian fluid in $\Omega_s$ is given from the solution of the Navier-Stokes equation and the fluid continuity equation.

$$\rho_{\mathrm{f}}\left(\mathbf{u}\cdot\nabla\mathbf{u}\right) = -\nabla p + \eta_{\mathrm{f}}\nabla^2\mathbf{u} \qquad \text{in } \Omega_s \qquad \text{(S1)}$$

$$\nabla\cdot\mathbf{u} = 0 \qquad \text{in } \Omega_s \qquad \text{(S2)}$$

in which $\rho_{\mathrm{f}}$ is the density of the fluid, $p$ the pressure, and $\eta_{\mathrm{f}}$ the viscosity of the fluid. Since an extremely dilute LiCl solution (30 mM) is considered in this simulation, the density and the viscosity of the fluid are assumed to be constant same as those of pure water (see **Table 1**). The parabolic velocity field of a fully-developed laminar flow is assumed at the inlet of the channel ($\Gamma_i$), where the average inlet velocity is $u_{avg}$. A square-shaped obstacles are placed within the channel to model the net-type spacer used in the experiment. The length of the square obstacle is 80 μm, corresponded to the hydraulic diameter of the cylindrically-shaped feed spacer threads which have the same diameter of 80 μm in the experiment. The surface-to-surface distance between two adjacent square obstacles is 220 μm. We placed buffer regions whose length is 400 μm near the inlet and outlet, where no square obstacles are placed to avoid unexpected numerical artifact by the presence of the obstacles near the inlet and outlet. No-slip and non-penetration boundary condition ($\mathbf{u} = \mathbf{0}$) are imposed on the channel wall and surface of the feed spacer ($\Gamma_w$). A pressure boundary condition is assumed at the outlet ($\Gamma_o$).

In the electrode domains ($\Omega_{ep}$ and $\Omega_{en}$), however, one should consider electrochemical reactions of lithium intercalation which provides the source term in the mass balance equation ($S_i$). We assumed that a Butler-Volmer form of electrochemical kinetics is hold in the lithium intercalation reaction as below:

$$i_{loc} = i_0\left(\exp\left(\frac{\alpha_a F\eta}{RT}\right) - \exp\left(-\frac{\alpha_c F\eta}{RT}\right)\right) \qquad \text{in } \Omega_{ep} \text{ and } \Omega_{en} \qquad \text{(S3)}$$

$$i_0 = F\left(k_c\right)^{\alpha_c}\left(k_a\right)^{\alpha_a}\left(c_{s,\max} - c_s\right)^{\alpha_a}\left(c_s\right)^{\alpha_c}\left(c_{\mathrm{Li}^+}/c_{\mathrm{Li}^+,\,\mathrm{ref}}\right)^{\alpha_a} \qquad \text{in } \Omega_{ep} \text{ and } \Omega_{en} \qquad \text{(S4)}$$

$$\eta = \varphi_s - \varphi_l - E_{eq} \qquad \text{in } \Omega_{ep} \text{ and } \Omega_{en} \qquad \text{(S5)}$$

$$S_i = \frac{v_{\mathrm{Li}^+} a_v i_{loc}}{nF} \qquad \text{in } \Omega_{ep} \text{ and } \Omega_{en} \qquad \text{(S6)}$$

in which $i_{loc}$ is the local current density, $i_0$ the exchange current density, $\alpha_a$ the anodic reaction rate coefficient in the electrode, $\alpha_c$ the cathodic reaction rate coefficient in the electrode, $\eta$ the overpotential, $k_a$ the anodic reaction rate constant in the electrode, $k_c$ the cathodic reaction rate constant in the electrode, $c_s$ the concentration of lithium in the solid particle phase (i.e., in the LMO particles), $c_{s,\max}$ the maximum concentration of lithium in the solid particle phase, $c_{\mathrm{Li}^+}$ the concentration of $Li^+$ ion in the liquid phase, $c_{\mathrm{Li}^+,\mathrm{ref}}$ the reference concentration of $Li^+$ in the liquid phase, $E_{eq}$ the equilibrium potential (see **Figure S2**), $v_{\mathrm{Li}^+}$ the stoichiometric coefficient of the reduction equation of $Li^+$, $a_v$ the active specific surface area [$m^{-1}$], and $n$ the number of electrons participating in the electrochemical reaction.

The concentration of lithium in the solid particle phase ($c_s$) at a specific time is given from the solution of an ordinary differential equation defined in the spherical coordinate system.

$$\frac{\partial c_s}{\partial t} = D_s \left[ \frac{\partial^2 c_s}{\partial r^2} + \frac{2}{r}\frac{\partial c}{\partial r} \right] \qquad (0 \le r \le r_p) \qquad \text{in } \Omega_{ep} \text{ and } \Omega_{en} \qquad \text{(S7)}$$

$$\frac{\partial c_s}{\partial r} = 0 \qquad at\ r = 0 \qquad \text{(S8)}$$

$$-D_s \frac{\partial c_s}{\partial r} = \frac{v_{\mathrm{Li}\theta} a_v i_{loc}}{nF} \frac{r_p}{3\varepsilon_s} \qquad at\ r = r_p \qquad \text{(S9)}$$

in which $D_s$ is the diffusion coefficient of lithium in the solid particle state, $r_p$ the radius of the LMO particle in the electrode, and $v_{\mathrm{Li}\theta}$ the stoichiometric coefficient of the reduction equation of lithium in the solid particle phase. The stoichiometric coefficients for lithium species, $v_{\mathrm{Li}^+}$ and $v_{\mathrm{Li}\theta}$, are derived from the electrochemical equation of the reduction process.

$$\mathrm{Li}^+ + \theta + v_{\mathrm{Li}^+} e^- \rightleftarrows \mathrm{Li}\theta \qquad \text{in } \Omega_{ep} \text{ and } \Omega_{en} \qquad \text{(S10)}$$

in which $\theta$ means an active site of the solid intercalation material. As single electron is participated in this reduction, it leads $v_{\mathrm{Li}^+} = 1$, while $v_{\mathrm{Li}\theta} = -1$ from the reverse reaction of Eq. (S10). As the stoichiometric coefficients are defined in the reduction reaction, $v_{\mathrm{Li}^+}$ and $v_{\mathrm{Li}\theta}$ are constant throughout the whole simulation

domain.

In the fully-blocking anion exchange membrane domain ( $\Omega_m$ ), $i_l$ is defined in a slightly different manners compared to the above cases, while $i_s = 0$ as non-conducting material is used in this domain.

$$\mathbf{i}_l = \mathbf{i}_m = -\sigma_m \nabla \varphi_m \qquad \text{in } \Omega_m \qquad \text{(S11)}$$

in which $\mathbf{i}_m$ is the electrolyte current density in the membrane, $\sigma_m$ the electrolyte conductivity in the membrane, and $\varphi_m$ the electrolyte potential in the membrane. It is assumed here that the charge transfer is solely done by conduction through the fixed electrolyte (=positive charge, in this case) in this domain, which is the case of the fully-blocking anion exchange membrane. We did not solved the Nernst-Planck equation in this domain, while the electrolyte current density ( $\mathbf{i}_l$ ) was matched with that solved in the adjacent domain.

In our numerical simulation, we impose proper initial and boundary conditions for the constant-current operation of our electrochemical lithium recovery system, as below.

***Initial conditions***

$$\varphi_l = 0,\ \varphi_s = E_{eq}(c_s),\ c_s = \mathrm{soc}_{0,\mathrm{int}} \cdot c_{s,\max} \qquad 0 \le x \le L_e \qquad \text{(S12)}$$

$$\varphi_l = 0,\ \varphi_s = 0 \qquad L_e < x < L_{tot} - L_e \qquad \text{(S13)}$$

$$\varphi_l = 0,\ \varphi_s = E_{eq}(c_s),\ c_s = \mathrm{soc}_{0,\mathrm{dei}} \cdot c_{s,\max} \qquad L_{tot} - L_e < x < L_{tot} \qquad \text{(S14)}$$

$$c_i = 0 \qquad L_e + L_s < x < L_e + L_s + L_m \qquad \text{(S15)}$$

$$c_i = c_{i,0} \qquad \text{otherwise} \qquad \text{(S16)}$$

in which $L_{tot} = L_e + L_s + L_m + L_s + L_e$ where the outer boundary of the negative electrode.

***Boundary conditions***

$$\mathbf{n} \cdot \mathbf{N}_\mathrm{i} = \mathbf{0},\ \mathbf{i}_l = 0,\ \mathbf{i}_s = \mathbf{I}_{cell},\ \varphi_l = 0 \qquad x = 0 \qquad \text{(S17)}$$

$$\mathbf{n} \cdot \mathbf{N}_\mathrm{i} = \mathbf{0},\ \mathbf{i}_l = 0,\ \mathbf{i}_s = \mathbf{I}_{cell} \qquad x = L_{tot} \qquad \text{(S18)}$$

$$\mathbf{n} \cdot \mathbf{N}_\mathrm{i} = \mathbf{0},\ \mathbf{n} \cdot \mathbf{i}_l = 0,\ \mathbf{n} \cdot \mathbf{i}_s = 0 \qquad \text{at the obstacle surface} \qquad \text{(S19)}$$

$$\mathbf{n}\cdot\mathbf{N}_{\mathrm{i}}=\mathbf{0},\ \mathbf{n}\cdot\mathbf{i}_{l}=0,\ \mathbf{n}\cdot\mathbf{i}_{s}=0 \qquad x=L_e+L_s\ or\ x=L_e+L_s+L_m \qquad \text{(S20)}$$

$$\varphi_l-\varphi_m=\frac{RT}{z_{\mathrm{Cl^-}}F}\ln\left(\frac{c_{\mathrm{Cl^-}}}{c_{m,\mathrm{Cl^-}}}\right) \qquad x=L_e+L_s\ or\ x=L_e+L_s+L_m \qquad \text{(S21)}$$

$$c_i=c_{i,0} \qquad \text{at the inlet of the separator} \qquad \text{(S22)}$$

$$\mathbf{n}\cdot D_i\nabla c_i=0 \qquad \text{at the outlet of the separator} \qquad \text{(S23)}$$

in which $c_{m,\mathrm{Cl^-}}$ is the concentration of the $Cl^-$ ion fixed in the anion exchange membrane.

***Mesh convergence test***

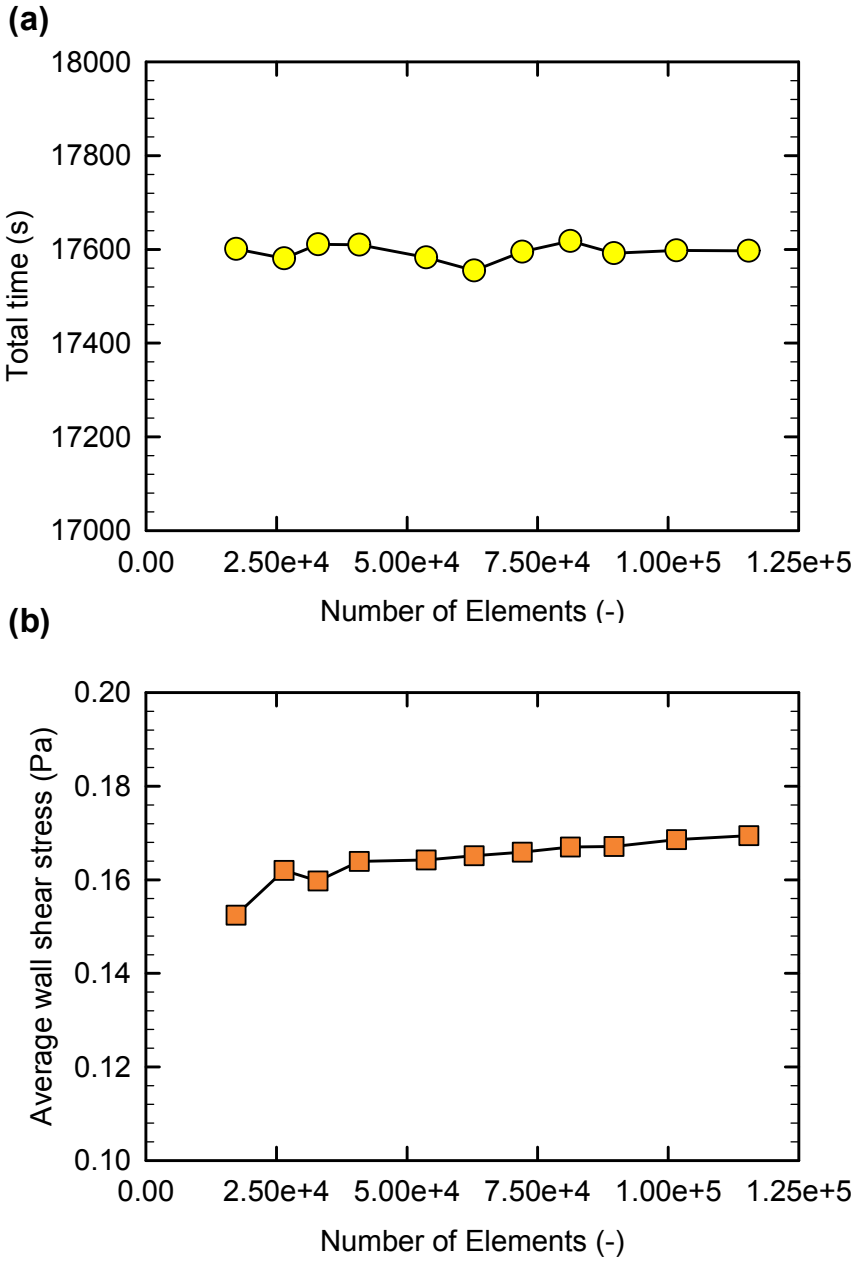


**Figure S3.** Mesh convergence test with (a) the total time and (b) the average wall shear stress on the positive electrode.

**Figure S3** summarizes the mesh convergence results in our simulation. It is revealed that refined computational mesh is needed to obtain average wall shear stress, however, the total time of the system operation (i.e., the time to reach to the limitation of voltage) is insensitive to the number of elements. We determine that 89,643 rectangular meshes are enough to be used in our simulation.

*Flow characteristics in the spacer-filled separator channel*

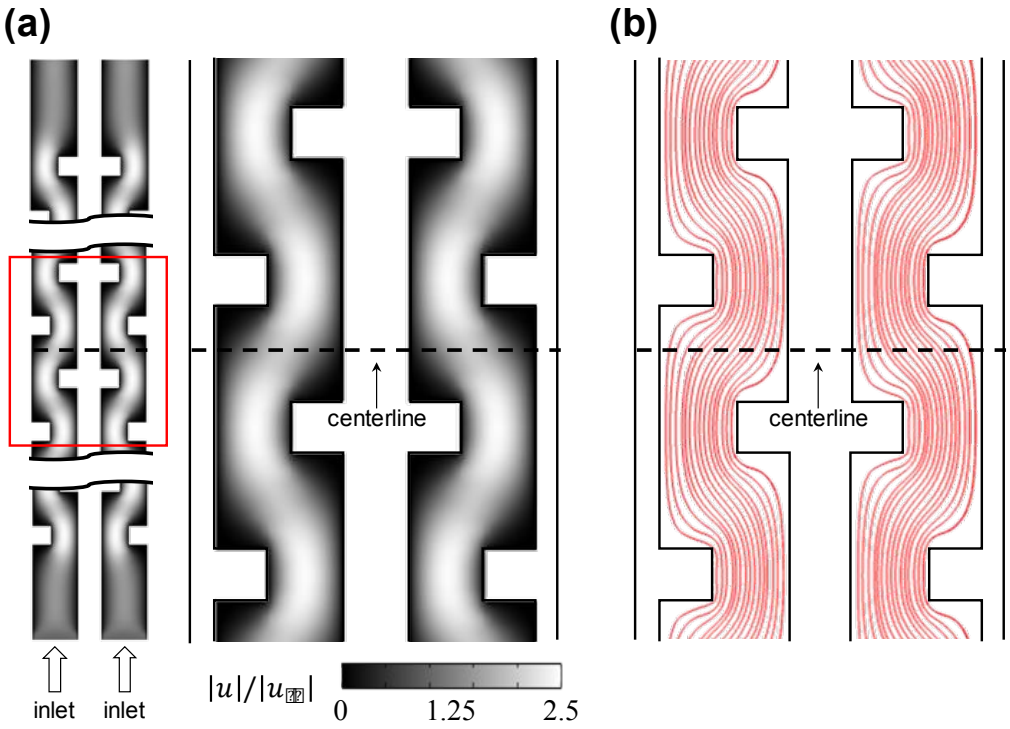


**Figure S4.** (a) Velocity contour plot of the flow in the system at the central region and (b) velocity contour line plot of the flow in the system. Flow rate was 1 ml/min for each channel.

**Figure S4** shows the velocity contour plots of the flow in the separator channel filled with spacer meshes. The zigzag configuration of the spacer meshes has two main effects on the flow. First, the flow rate is increased up to 2.5 times the inlet flow rate as shown in **Figure S4a**. The feed solution in contact with the electrode is renewed quickly compared to the absence of the spacer mesh and it is advantageous for mass transport of $Li^+$. Secondly, the vertical flow direction is altered by the presence of spacer meshes as shown in **Figure S4b**, which is beneficial for the mass transfer in the separator channel.

*Effect of spacer mesh on the concentration distribution*

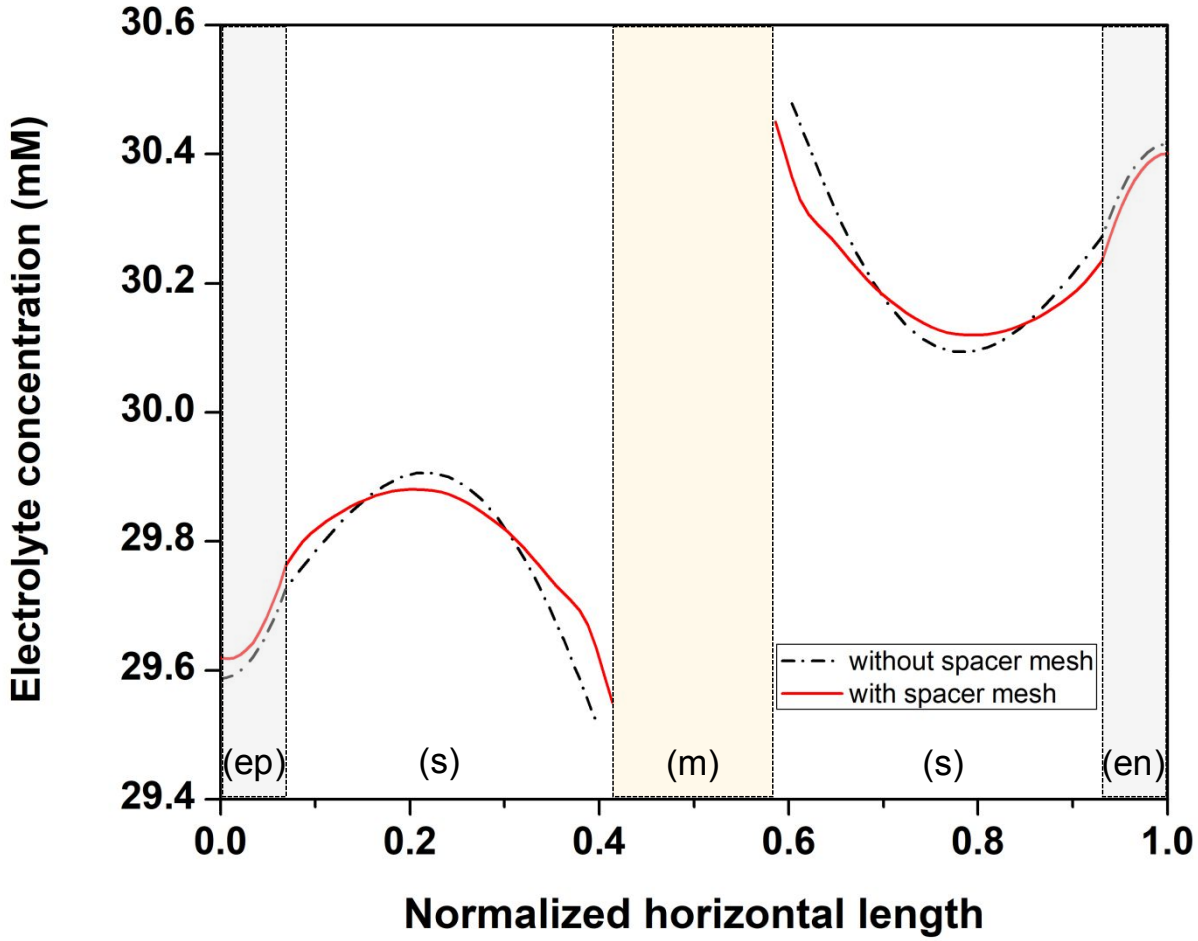


**Figure S5.** Electrolyte concentration profile with normalized horizontal length at the center of the system with (red solid line) and without spacer (black dash dot line) mesh at the step 1 (representative current: 0.5 mA).

**Figure S5** shows the electrolyte concentration profile with and without spacer mesh in the cross-section perpendicular to the flow direction. In both case, the shape of the profiles is parabola, indicating concentration polarization in the separator channel. In the presence of the spacer mesh, the difference between the maximum and minimum concentration is smaller than in the absence of the spacer mesh. In other words, the concentration polarization can be alleviated by the spacer mesh in the flow-type electrochemical ELR system.